

Original Article

# Design and Analysis of a 2-Port Multiple Antenna System with Slotted Ground and Square Split Ring Resonator at Millimeter Wave Frequency

Priyadarshini K Desai<sup>1</sup>, S. Bindu<sup>2</sup>

<sup>1,2</sup>Department of ECE, BNMIT, VTU, Karnataka, India.

<sup>1</sup>Corresponding Author : priyadarshini.p.r@gmail.com

Received: 04 October 2022

Revised: 08 November 2022

Accepted: 18 November 2022

Published: 30 November 2022

**Abstract** - The current wireless communication technologies demand high data rates, seamless connectivity and low latency. The Multiple Antenna system is one of the primary technologies that promise a high data rate. This system performance is improved when the antennas are highly isolated and mutual coupling among the antenna elements is low. In this article, the performance of a 2-port Multiple antenna system is enhanced with two decoupling strategies, namely, Slotted Ground (SG) and Square Split Ring Resonator-metamaterial (SSRR- metamaterial) with the slotted ground. The antenna system is assessed through the Envelope Correlation Coefficient(ECC), Diversity Gain (DG), and Mean Effective Gain for both decoupling methods. The obtained value of ECC for SSRR-metamaterial with the SG and with SG alone is 0.00024 and 0.004, respectively. The results indicate that the SSRR-metamaterial with the SG offers superior isolation between antenna elements, thereby improving the performance of the overall antenna system.

**Keywords** - Microstrip Patch Antenna, Millimeter-wave, Multiple Antenna System, Slotted Ground, Square Split Ring Resonator.

## 1. Introduction

Wireless communication technologies have evolved from their first 1G to the current 5G. Every generation has provided better communication quality in terms of connectivity, data rate and latency. The betterment is achieved due to changes in the operating frequency and the new system's design that can operate at the required frequency. The current fifth generation promised a high data rate, measured in gigabits per second. It is one of the main requirements that must be satisfied by the existing and next wireless technologies. This need can be met by implementing a multiple input, multiple output system. If the radiating element displays strong isolation between them, the Multiple-Input-Multiple-Output system will function properly. As the present 4G-LTE band is fully utilised and the millimeter-wave band frequency is the next possible frequency band, the next-generation wireless technology necessitates that the devices function at a new frequency band as well. There has been a surge in interest in millimeter-wave gadget design.

Antennas are a crucial component of wireless communication, and it is well known that as working frequencies rise, antenna size decreases. The construction of a small and compact antenna system will have the primary

benefit of size reduction. Multiple-Input-Multiple-Output was created because a single element can accommodate the need for a significant data rate. A single antenna is converted into an NxN antenna structure.

The Multiple Antenna system performances is low if the isolation between the elements is not maintained high. One method to increase the isolation is to add a decoupling structure during the design of the Multiple Antenna system. Therefore, building multiple input multiple output antenna systems with good radiating element isolation is crucial. To lessen the contact between antennas, a number of approaches have been developed, including the use of metamaterials, parasitic elements, and energy-band gap structures.

## 2. Literature Survey

The microstrip patch antenna is designed to operate in Ultra-wideband (UWB), and bandwidth enhancement is achieved by changing its shape [1]. The planned antenna is transformed to 2x2 MIMO, and the decoupling structure is a meta-surface composed of SRR. The measurement shows a transmission coefficient of -43dB. ECC and diversity gain are respectively 10dB and 0.07. The findings demonstrated that, at UWB frequency, the use of metamaterials increased the isolation between radiating elements.



A unique metamaterial absorber in the form of a flower has been created and is being used as a decoupling structure [2]. The 5.5 GHz WiMAX spectrum is intended for the MIMO antenna technology. A metamaterial absorber with a four-element array is intended to form a line between two radiating elements. A -33dB isolation has been attained. ECC, DG, and TARC were the Multiple Antenna performance metrics assessed. The obtained ECC and DG values are 0.004 and 10 dB, respectively. However, the radiation efficiency was 68.03%. Due to the partial ground structure, the radiation efficiency was reduced.

For the purpose of reducing mutual coupling in multiple antenna systems, a Meta surface antenna array decoupling technique is used [3]. A two-element MIMO antenna array is suspended by a meta-surface composed of SRR with a 5.8GHz frequency configuration. At the desired frequency band, isolation is -27dB. The obtained ECC is 0.08

Using a hybrid electric and magnetic coupling structure improves the isolation in MIMO antenna systems [4]. The operating range of the MIMO antenna system is 2.3-2.8GHz. A Split ring resonator is a structure that uncouples the radiating element. With a split ring structure, a -30 dB decoupling factor was achieved. From 2.3GHz to 2.9GHz, the ECC is less than 0.005, which is extremely modest. The MIMO antenna's channel capacity loss, which ranges from 1.28 to 16.55 bps/Hz, is also assessed. The sub-6GHz frequency spectrum is the intended range for the MIMO system.

Broadband SCS for broadcasting and communications applications is built with a quad-band antenna with high isolation MIMO [5]. The dual PIFA and the addition of a self-complementary structure produced a quad-band. The developed antenna exhibits good impedance matching at WLAN at 2.4GHz and 5.15GHz, L-band, and UHF. First, the antennas were oriented so that they were orthogonally aligned. Next, a connecting line was utilised near the feed point, which essentially served as a band-stop filter at 2-GHz. Finally, a connecting plane is used on the bottom side of the antenna. All three approaches were utilised for an antenna operating at three separate frequencies. The achieved isolation of the antenna elements is -30dB.

An extremely small MIMO antenna system for WiMAX and WLAN is designed and investigated [27]. Its radiating elements were arranged orthogonally. A Y-shaped parasitic element is employed between the orthogonal elements in addition to orientation. The system is 20mm by 20mm in size. With 80% radiation efficiency, the transmission coefficient is -43 dB, and the ECC is roughly 0.004.

According to a survey [7] on massive MIMO's ability to support the next generation of wireless communication technology, some of its advantages include a ten-fold

increase in capacity and a concomitant 100-fold increase in radiated energy efficiency. It is said that adopting a significant number of antennas will enable a massive gain in energy efficiency.

The phase shift concept creates a unique decoupling structure [8]. A shorting pin and a half-wave microstrip line make up the innovative construction. Due to the provision of an additional signal line, the mutual coupling between the nearby patch antennas is minimised. A 7-8dB improvement in isolation exists between the two patch elements at 3.16GHz, the frequency of operation.

When employed in antenna design, the notion of characteristic modes is used to examine the behaviour of a defective ground structure [9]. A methodical process is used to analyse and determine whether the isolation may improve. Two 4-element and one 2-element MIMO antenna systems with individual monopole and PIFA elements were constructed for the case study. The paper concluded that an 11dB isolation increase is possible with the addition of DGS.

Two other types of feed lines, one based on a substrate-integrated cavity and the other on surface plasmon polarisation, are also used to improve isolation [10]. Broadband decoupling is made possible by the SIW and SSP's high-pass and low-pass feeding networks.

A T-junction power combiner/divider is designed to excite a 2-element array [11]. To increase isolation, defective earth with shapes like rectangles, circles, and zigzags is inserted into the soil. The designed antenna operates in the 25.5-29.6 GHz mm-wave band. 8.3 dB is the obtained peak gain. ECC, MEG, and DG are estimated for the designed MIMO antenna for varied form DGS structures.

For use with UWB, a single negative metamaterial monopole antenna is created [12]. The SNG metamaterial is put into the single monopole antenna. By increasing the bandwidth from 3.08GHz to 14.1GHz, an average gain of 4.54dB was provided.

An antenna is used as the microwave oven's temperature sensor [13]. The sensor node, which serves as a temperature-detecting element, is where the UWB antenna is mounted.

The resonance frequencies for metamaterial are 250MHz, 200MHz, 150MHz, and 50MHz [28]. The main function of metamaterial is to act as a sensor to detect different chemical samples with a strong dielectric response.

The metamaterial is employed as the superstrate in a split ring resonator [15]. When a patch antenna is loaded with superstrate, the gain increases by 7.6dB at 5.9GHz, but the bandwidth remains unchanged. Gain with metamaterial as superstrate is the antenna parameter that has been improved.

A superstrate that uses a split ring resonator at UWB frequency has been developed [16]. The analysis of a split ring resonator with more rings and more space between them has been done. The patch antenna demonstrates the increase in bandwidth with a loaded SRR superstrate.

Exclusive investigation of the s-band and x-band gap-linked hexagonal splits ring resonator metamaterial [17]. The 10mmx10mm GCHSRR is printed on the dielectric material FR-4. The developed metamaterial displayed negative permittivity and permeability in the S-band and X-band spectrums. At 4.27 GHz, 5.42 GHz, and 12.40 GHz, the metamaterial's absorption peaks were found to be 99%, 98%, and 82%, respectively. The proposed GCHSRR is appropriate for microwave applications due to its strong absorptance.

At 15GHz, a brand-new single negative metamaterial made of concentric rings and crossing lines is designed [18]. At several frequency bands, the developed metamaterial exhibited a single negative behavior. The patch is positioned below the metamaterial. With the introduction of metamaterial into the ground plane, bandwidth and impedance matching increase from 2GHz to 20GHz.

A 3-port multimode antenna is used as a unifying element in designing and analysing a small 108-element base station antenna array [29]. The 75mmx75mmx14.8mm three-layer with aperture couple feed made up the three-port multimode antenna. The middle patch is a square ring patch connected to port-1 and port-2. The gain obtained through the unit element was 6.5dB, and the impedance bandwidth of 254MHz (2.248GHz-2.486GHz) and 238MHz (2.248GHz-2.486GHz) when port-1 and port-2 were excited. The upper patch is a square patch with a slot connected to port-3. The elements' mutual coupling is kept at -14 dB.

Additional base station antenna testing is needed for the MIMO-OFDM downlink system's multiuser urban street grid scenario. Singular value spread and DPC sum capacity for the proposed 108-element base station antenna converge to 7dB and 11.6bps/Hz at 10dB SNR for a 4-user case using the same frequency and time resource.

The s-parameter and far-field patterns are primarily used to analyse the correlation coefficient of the MIMO antenna system. If the antenna element's radiation efficiency is high, the obtained value of CC is notable. The CC analysis considers the N-port's radiation efficiency and the s-parameter [20]. The effect of beam tilt on the correlation coefficient is also explored.

Microstrip patch antennas are integrated with metamaterial to improve their functionality [21]. To increase the impedance bandwidth, the patch is loaded with a complementary split ring resonator structure close to the

feedline. The CSRR in the ground structure, which also had a flaw, was bigger than the CSRR loaded with the patch. The entire building is made to function at 2.4GHz Wi-Fi frequency.

A 1.7789 GHz and 2.459 GHz dual-band terahertz metamaterial absorption device is created [30]. A metallic mirror and two similar square patches make up the absorption device. There is an insulating material positioned between the patch and the metallic mirror. It is possible to realise two resonance peaks with almost complete absorption. Different field creation techniques resulted in the Q-factor of 6.9156 and the ultra-high Q-factor of 296.28 being produced.

A millimeter-Wave energy bandgap structure is intended to function [23]. A conventional uniplanar EBG unit cell is transformed into an EGB unit cell by adding two connecting bridges and etching two slots. The EBG's size is 78% smaller than a typical unit. The massive antenna array at 60GHz millimetre wave frequency can use the planned EGB's performance as a decoupling device.

The performance of a 2-port MIMO antenna with two isolation approaches is performed in the suggested study. In section I, the design and analysis of the feed line and the solitary element microstrip patch antenna are discussed. The 3.725mm x 4.474mm microstrip patch antenna is built of copper with a thickness of 0.017mm and is etched on the dielectric substrate Rogger 5880, which has a relative permittivity of 2.2 and a thickness of 0.5mm. The Rogger 5880 is employed because it gives low loss when utilised at millimetre frequency. Dimensions of the ground plane are 15 mm x 15 mm x 0.017 mm. A single microstrip patch antenna yields a reflection coefficient and gain of -25dB and 7.67dB, respectively.

### 3. Proposed Design and Analysis of Multiple Antenna System

In this manuscript, 2-port Multiple antenna system is designed. The comparison study of the system is carried out using two decoupling strategies. Initially, a single microstrip patch antenna is designed to resonate at 24GHz; the details are discussed in section 3.1. Section 3.2 give an introduction to the performance metrics that are used in multiple antenna system assessments. The microstrip patch antenna is converted into 2-port Multiple antenna system. The slot is introduced in the antenna system's ground plane, and a detailed analysis is explained in section 3.3. The design of Square Split Ring Resonator-metamaterial and its characteristics is explained in section 3.4. Section 3.5 discusses the design and performance of the SSRR-metamaterial loaded 2-port Multiple Antenna system. Fitting the 2-port Multiple Antenna within the same 15mmx15mm dimension and achieving high isolation is the primary goal of the effort. In the CST microwave studio, the single

microstrip patch antenna, the 2-port Multiple Antenna and Square Split Ring Resonator are simulated.

### 3.1. Design and Study of Microstrip Patch Antenna

A dielectric substance is often placed between the two metallic patches in a microstrip patch antenna. The radiating patch is the metallic patch that is located beneath the substrate. The substrate typically has a dimension of  $\lambda/2$ . When working at a higher frequency, a dielectric material is chosen with a low substrate loss. The Rogger 5880 substrate is chosen because it has a relative permittivity of 2.2 and a thickness of 0.5mm and is intended to work at 24GHz. The following equation (1)-(5) is used to compute the patch antenna's width and length.

$$W_p = \frac{c}{2f_0 \sqrt{\frac{\epsilon_r + 1}{2}}} \quad (1)$$

$$L_p = L_{eff} - 2\Delta L \quad (2)$$

$$\Delta L = 0.412t_s \frac{(\epsilon_{eff} + 0.3)\left(\frac{W}{t_s} + 0.264\right)}{(\epsilon_{eff} - 0.258)\left(\frac{W}{t_s} + 0.8\right)} \quad (3)$$

$$L_{eff} = \frac{C}{2f_0 \sqrt{\epsilon_{eff}}} \quad (4)$$

$$\epsilon_{eff} = \frac{\epsilon_r + 1}{2} + \frac{\epsilon_r - 1}{2} \left[1 + 12 \frac{t_s}{W}\right]^{-1/2} \quad (5)$$

Using the calculation mentioned above, the microstrip patch antenna's dimensions are  $W_p = 4.2\text{mm}$  and  $L_p = 4.1\text{mm}$ . The antenna is designed to have an optimal length and width to resonate at the necessary frequency of 24GHz.

The attachment of the antenna to its feed line is crucial since a microstrip line is employed as the feed line. According to equation (6), the microstrip line's characteristic impedance depends on the line's height, width, and permittivity.

$$Z_c = \frac{120\pi}{\sqrt{\epsilon_{eff}} \left[ \frac{W_f}{t_s} + 1.393 + 0.667 \ln \left( \frac{W_f}{t_s} + 1.44 \right) \right]} \quad (6)$$

With its standing for the height of the dielectric substrate,  $W_f$  for the line's width, and  $\epsilon_{eff}$  for the substrate's effective permittivity. To achieve adequate impedance matching, the feed width is parametrically changed. Figure 1 shows the designed microstrip patch antenna. As seen by S11 in Figure 2, a 0.5mm feed width provided better impedance matching. Table 1 displays the planned microstrip patch antenna's dimensions. The far-field pattern of the designed antenna is shown in Figure 3

**Table 1. Microstrip Patch Antenna dimension**

Antenna Structure	Parameter (Symbol)	Value (mm)
Metal Ground	Length ( $L_G$ )	15
	Width ( $W_G$ )	15
	Thickness ( $t_G$ )	0.017
Dielectric Substrate	Substrate_Width ( $W_s$ )	15
	Substrate_Length ( $L_s$ )	15
	Substrate_Thickness( $t_s$ )	0.5
Rectangular Patch	Patch_Width ( $W_p$ )	4.74
	Patch_Length ( $L_p$ )	3.84
	Patch_Thickness ( $t_p$ )	0.017

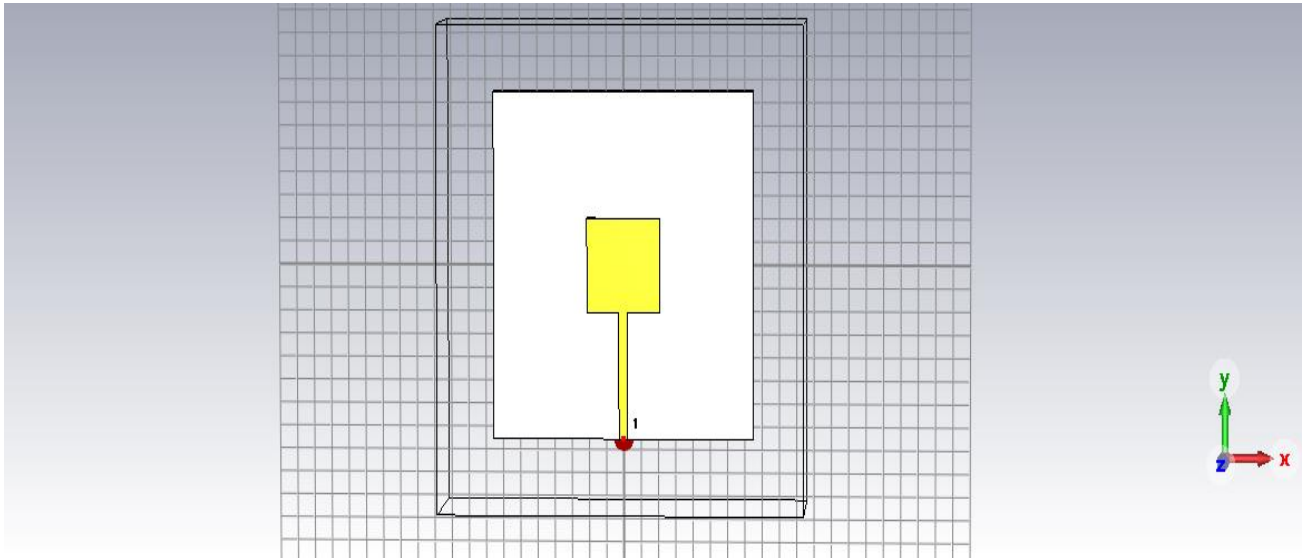


**Fig. 1 Proposed Microstrip Patch Antenna**

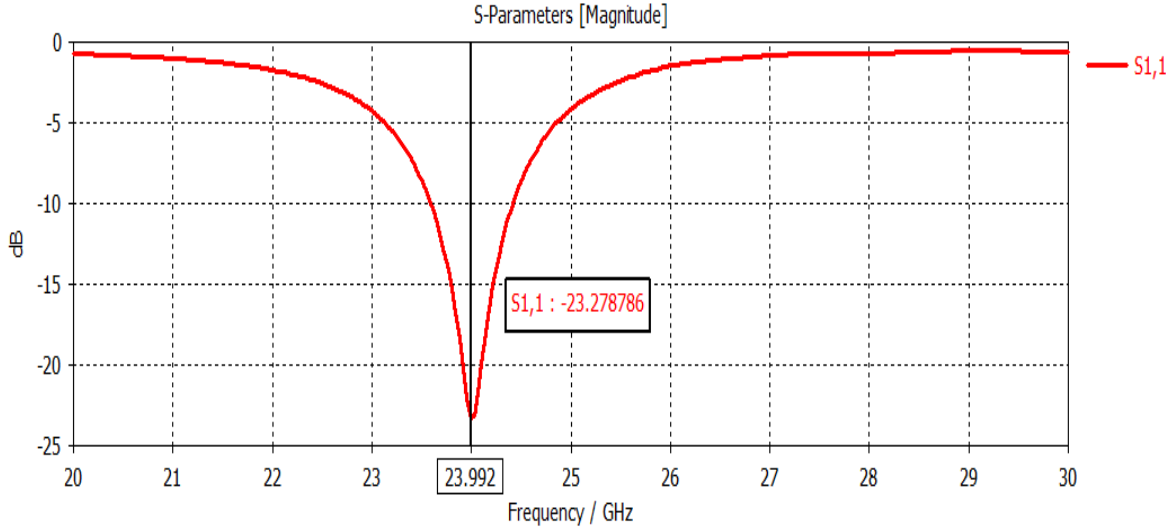


Fig. 2 Reflection Coefficient (S11) v/s Frequency Plot of the Microstrip Patch Antenna.

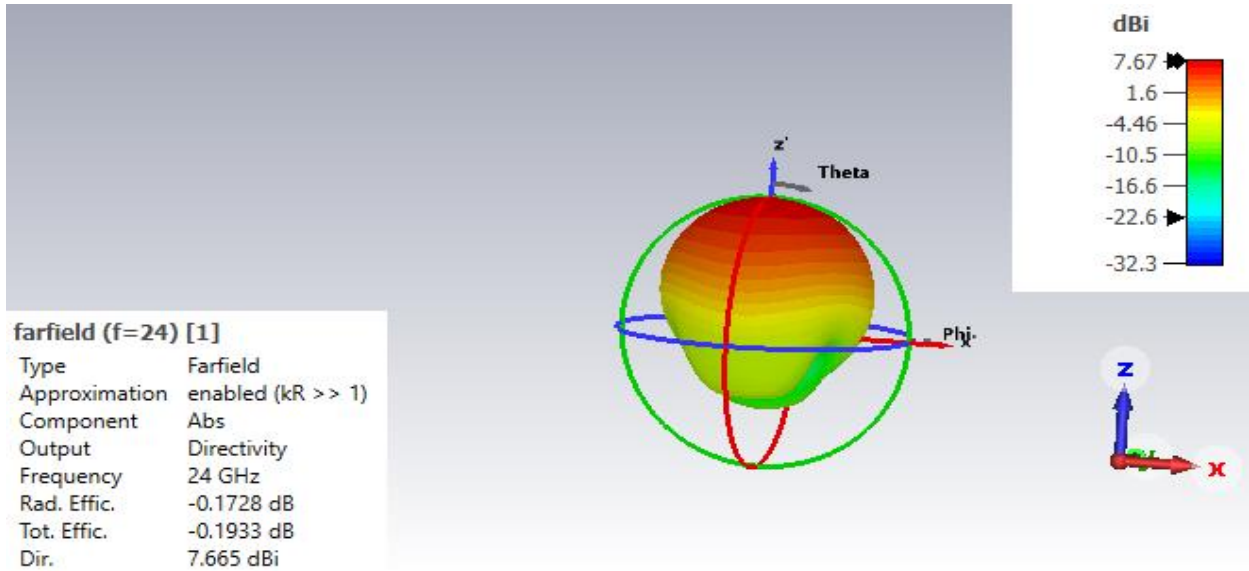


Fig. 3 The far-filed pattern of the Microstrip Patch Antenna

### 3.2. Multiple-Input-Multiple-Output Performance Metrics

The performance of the Multiple Antenna System can be evaluated using a variety of metrics; in this work, Envelope Correlation Coefficient (ECC), Diversity Gain (DG), and Mean Effective Gain (MEG) are used to assess the performance of the proposed multiple antenna system

In Multiple antenna systems, the radiating elements must be highly isolated, and ECC measures the correlation between the radiating elements. The correlation is observed both in terms of Field pattern and S-parameters. ECC has been assessed in this work employing equation (7) (where i and j are antennas, and N is the total number of antennas taken under consideration) via S-parameters between

components of the shown Multiple Antenna System.

$$\rho_e = \frac{|\sum_{n=1}^N S_{i,n}^* S_{n,j}|^2}{\prod_{k=(i,j)} 1 - \sum_{n=1}^N S_{i,n}^* S_{n,k}} \quad (7)$$

Mean Effective Gain (MEG) of any two antennas in a Multiple Antenna System must be -3dB to meet the power standards. Basically, MEG is the ratio of the antenna's average absorbed power to the average incident power. In a Multiple Antenna system, mean effective gain measures or examines the power imbalance over a channel or propagation medium. It is a crucial metric for measuring the effectiveness of Multiple Antenna Systems. The equation is used to perform the MEG calculation (8)

$$MEG = \int_0^{2\pi} \int_0^\pi \left[ \frac{XPR}{1+XPR} G_\theta(\theta, \varphi) P_\theta(\theta, \varphi) + \frac{XPR}{1+XPR} G_\theta(\theta, \varphi) P_\theta(\theta, \varphi) \right] \sin\theta \, d\theta \, d\varphi \quad (8)$$

$G_\varphi$  and  $G_\theta$  are the power gain patterns of the antenna when  $\theta$  is varied, and  $\varphi$  is constant in the case of  $G_\varphi$  and vice versa  $G_\theta$ .  $XPR=0$  for an outdoor uniform propagation environment.

Diversity Gain describes the degree to which Multiple Antenna System outperforms SISO (Single Input, Single Output). It can be calculated using relation 9.

When using maximum-ratio combining, the maximum diversity gain is 10 at the 1% probability level, and  $e_p$  is the diversity gain reduction factor resulting from the signal

correlation between the two antennas ( $e$  is the envelope correlation coefficient).

$$DG = 10 \times e_p = \sqrt{(1 - |0.99e_{ij}|)^2} \quad (9)$$

### 3.3. Design and analysis of 2-Port Multiple Antenna with a Slotted Ground Structure Study

The intended microstrip patch is often transformed into a 2-port Multiple Antenna System. Figure 4 depicts the top and bottom views of a 2-port Multiple Antenna System with a slotted ground construction. The slot, having a dimension of 2 mm x 12 mm (x, y), is introduced in the ground plane. The current flow is typically interrupted when a slot is introduced, increasing the isolation between the radiating elements and thereby minimising mutual coupling.

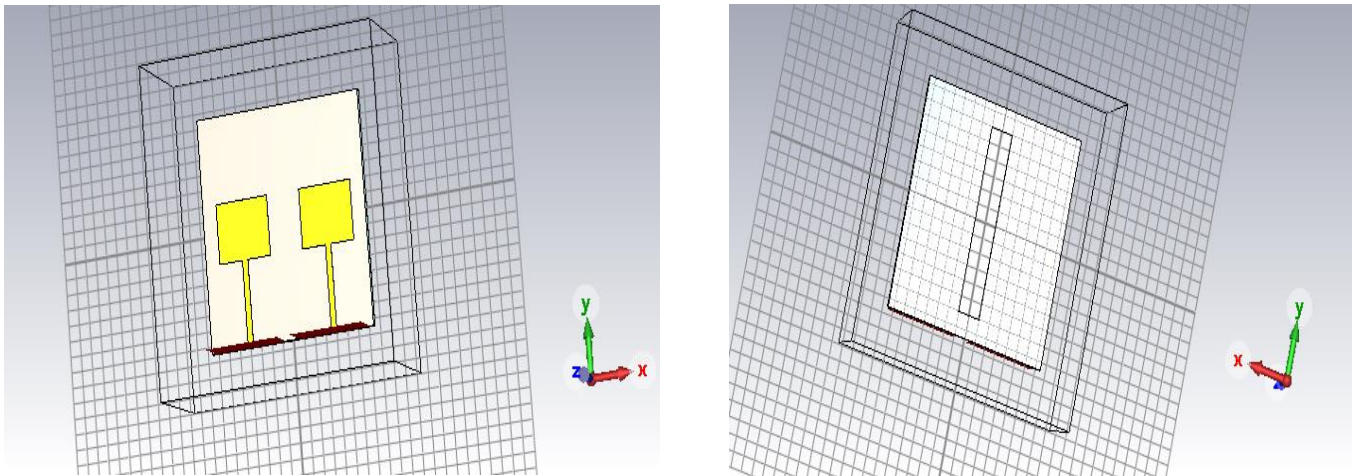


Fig. 4 A 2-port Multiple Antenna System with Slotted Ground (a)Top view (b) Bottom view

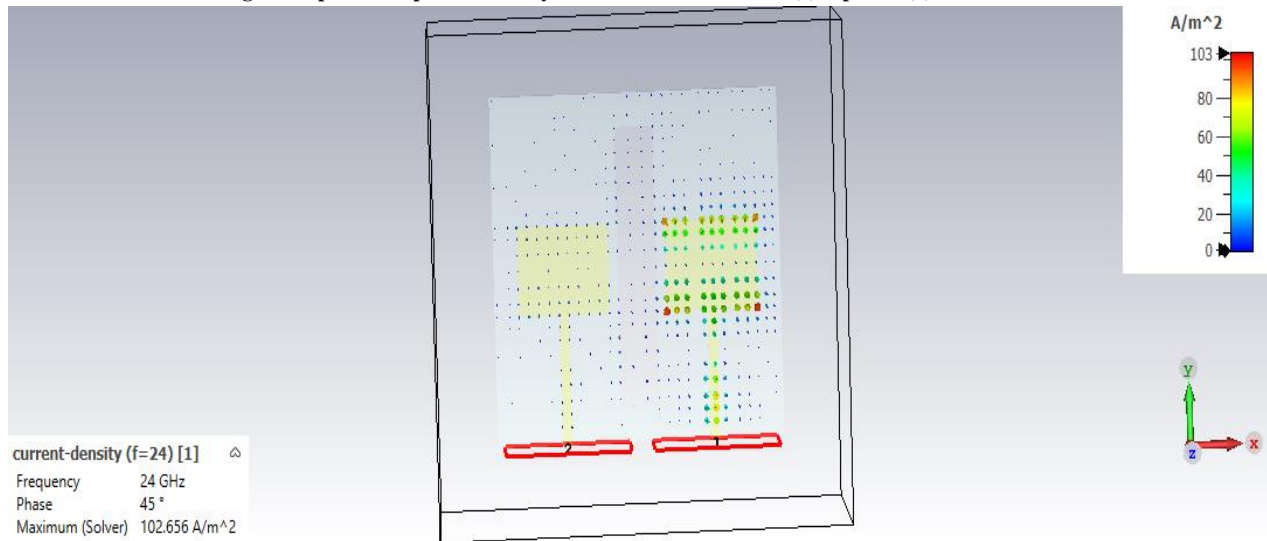


Fig. 5 Surface Current Density of 2-port Multiple Antenna System with Slotted Ground Structure

The surface current observation from Figure 5 shows that when microstrip patch antennas are excited, there is a discontinuity in the surface current flow. It occurs because there is a defective ground structure present. As a result, the isolation between the parts grows, improving the performance of the multiple antenna system.

The simulated far-field pattern of the 2-port Multiple antenna system is shown in Figure 6. It can be observed that the major lobe direction is along  $5^\circ$  for both the radiating elements for  $\phi = 0$  plane. It indicated a very minor change in the pattern with the presence of a slotted ground structure.

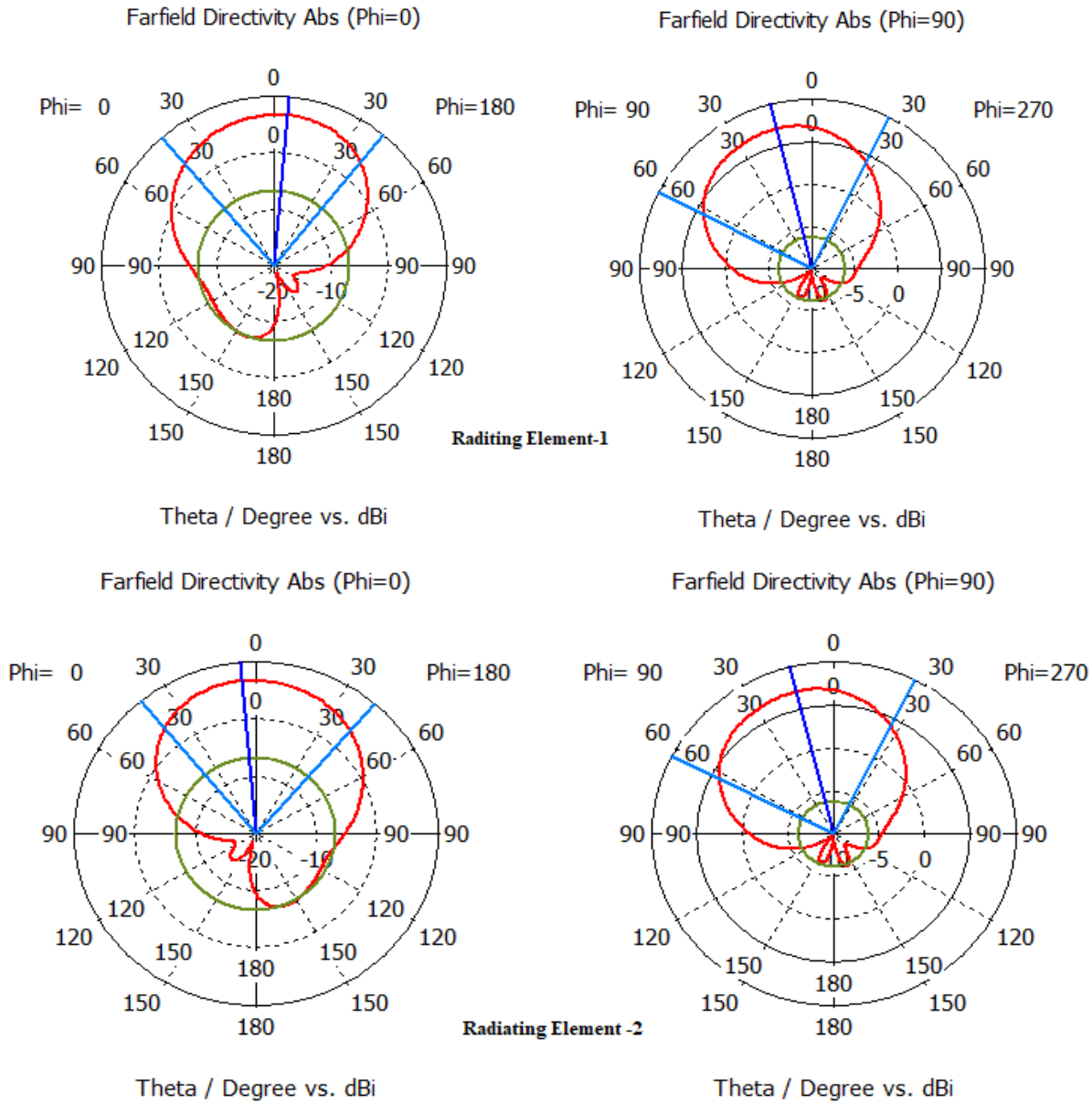


Fig. 6 Far Field Pattern of 2-port Multiple Antenna System with Slotted Ground Structure

The transmission coefficient is  $-20.86$  dB, and the antenna is spaced  $\lambda/4$  apart, as depicted in Figure 7. By using far-field patterns, the envelope correlation coefficient is assessed. Figure 8 shows that the obtained value of ECC is 0.004, which is less than the usual value of 0.005 needed to maintain the minimum correlation between the Multiple

Antenna System. The Multiple Antenna system's diversity gains must be 10dB. With the proposed Multiple Antenna system with a Slotted Ground decoupling structure, the diversity gain measured in Figure 9 is around 9.99dB. Figure 10 displays the Mean Effective Gain of the 2-port Multiple Antenna System with Slotted Ground, which is  $-3$ dB.

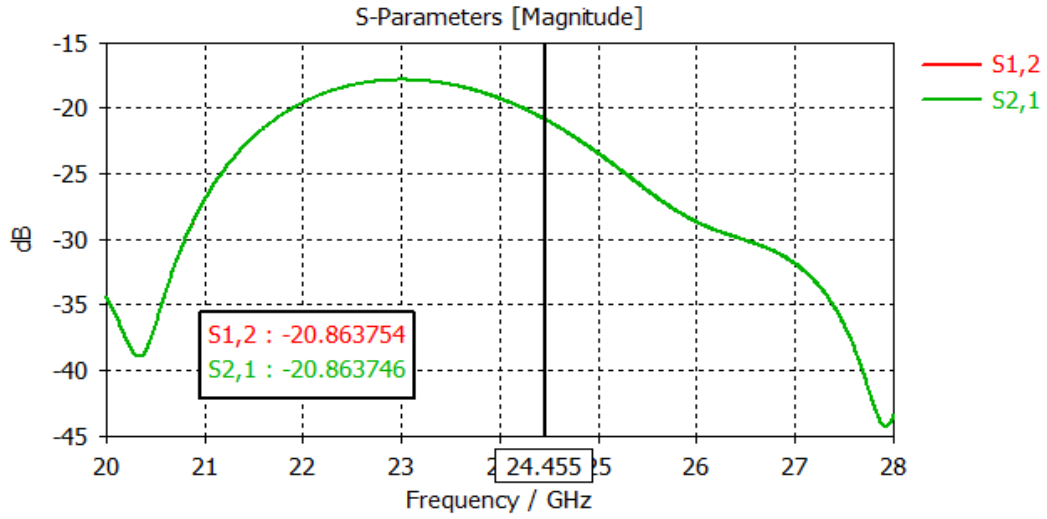


Fig. 7 Transmission Coefficient (S12, S21) of 2-port Multiple Antenna System with slotted ground

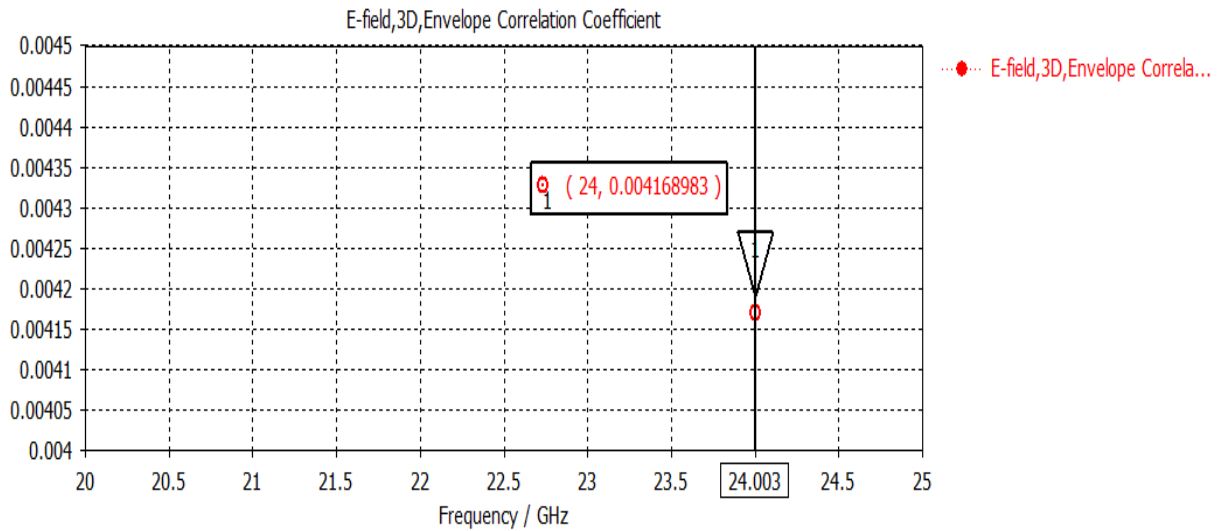


Fig. 8 ECC v/s Frequency of 2-port Multiple Antenna System with slotted ground

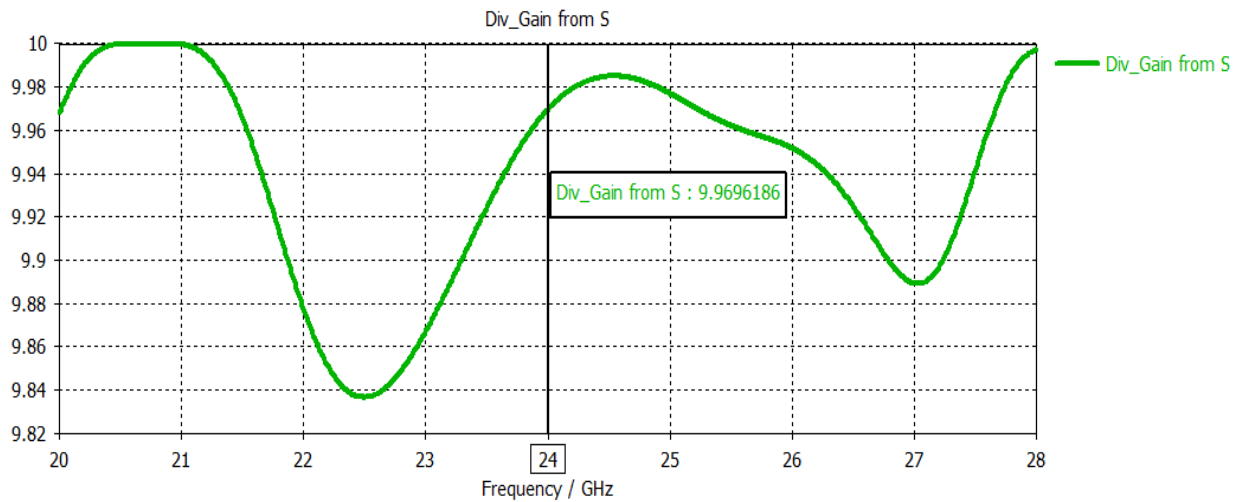


Fig. 9 Diversity Gain v/s Frequency of 2-Port Multiple Antenna System with Slotted Ground.

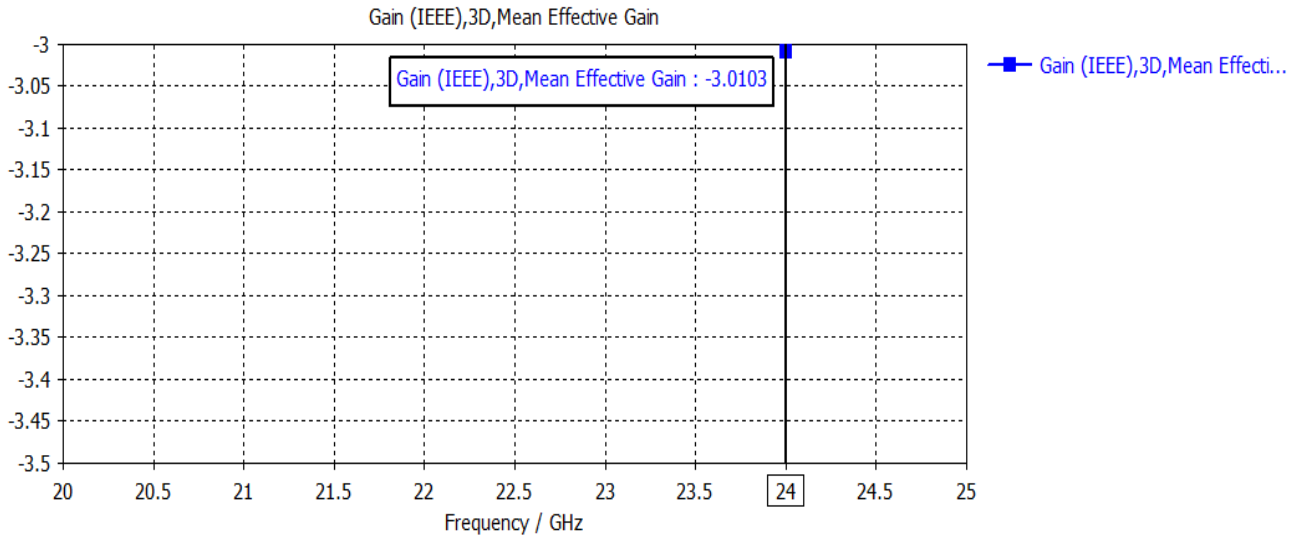


Fig. 10 Mean Effective Gain v/s Frequency of 2-Port Multiple Antenna System with Slotted Ground.

### 3.4. Square Split Ring Resonator-Metamaterial Design and Analysis

An SSRR-metamaterial comprises two concentric metallic rings that have been etched onto a dielectric substrate, with slits etched on the opposing side. The RT5880 substrate, which has a thickness of 0.5mm, is used to build the SSRR-metamaterial unit cell. The unit cell displayed the metamaterial property was 1.6 mm × 1.6 mm in size. Table 2 lists the SSRR's dimension

Table 2. Split Ring Resonator Dimension

SSRR-Structure	Parameter (Symbol)	Value (mm)
Outer Metallic Ring	Width ( $W_1$ )	0.11
	Length ( $L_1$ )	1.2
	Thickness (t)	0.017
Dielectric Substrate	Width ( $W_s$ )	1.6
	Length ( $W_s$ )	1.6
	Height (h)	0.5
Inner Metallic Ring	Width ( $W_2$ )	0.11
	Length ( $L_2$ )	1.2
	Thickness (t)	0.017

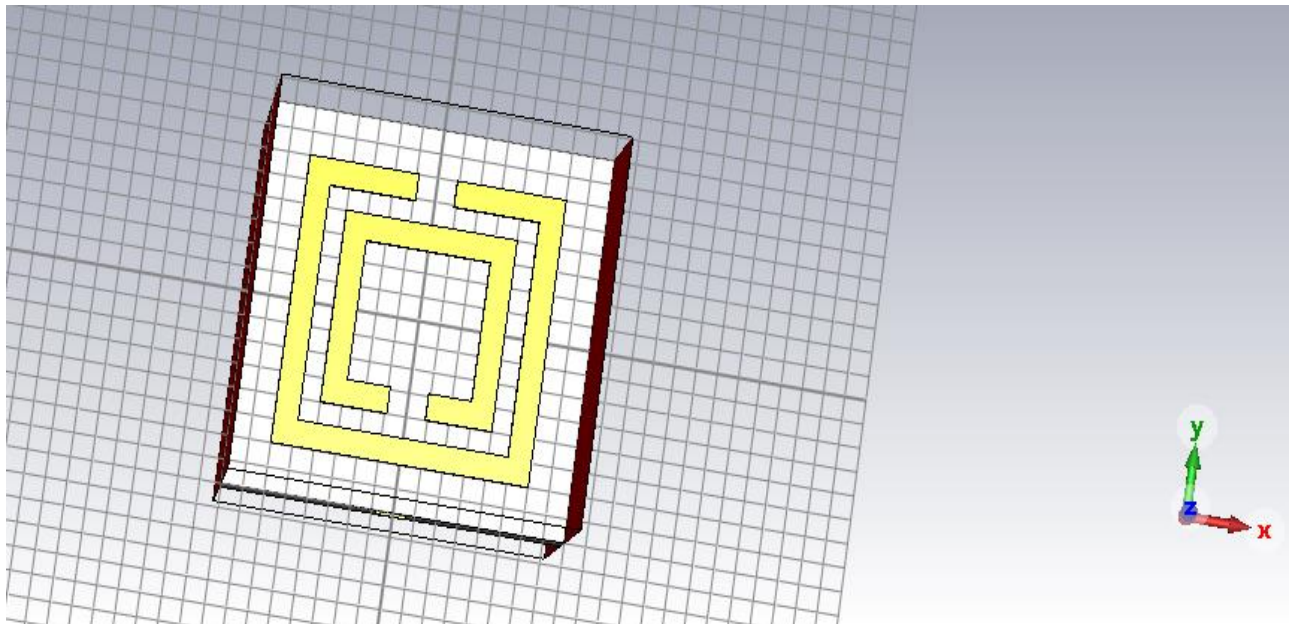


Fig. 11 Designed SSRR-metamaterial at 24GHz

Equation (10) can be used to determine the resonance frequency of SSRR metamaterial, as stated in [24-25]:

$$f = \frac{1}{2\pi\sqrt{LC}} \quad (10)$$

Metamaterial characteristics are examined using S-parameters. Refractive index (n), impedance permittivity, and permeability of SRR are determined using the s-parameters and equations (11–14).

$$n = \frac{1}{kd} \cos^{-1} \left[ \frac{1}{2S_{11}} (1 - S_{11}^2 + S_{21}^2) \right] \quad (11)$$

$$z = \sqrt{\frac{(1 + S_{11}^2) - S_{21}^2}{(1 - S_{11}^2) - S_{21}^2}} \quad (12)$$

$$\epsilon = \frac{n}{z} \quad (13)$$

$$\mu = \frac{n}{z} \quad (14)$$

The metamaterial layer function as an effective resonator with a high Q-factor. This property of the metamaterial makes it helpful for serving as an isolating component in the Multiple Antenna System. The 1.6mm x 1.6mm SSRR-metamaterial unit cell is created on a 0.2mm thick Rogger 5880 substrate, as seen in Figure 11. The magnitude curve of the S-parameter is shown in Figure 12 shows that the intended SRR displays a phase change at roughly 24GHz. The phase plot of the S-parameter is shown in Figure 13.

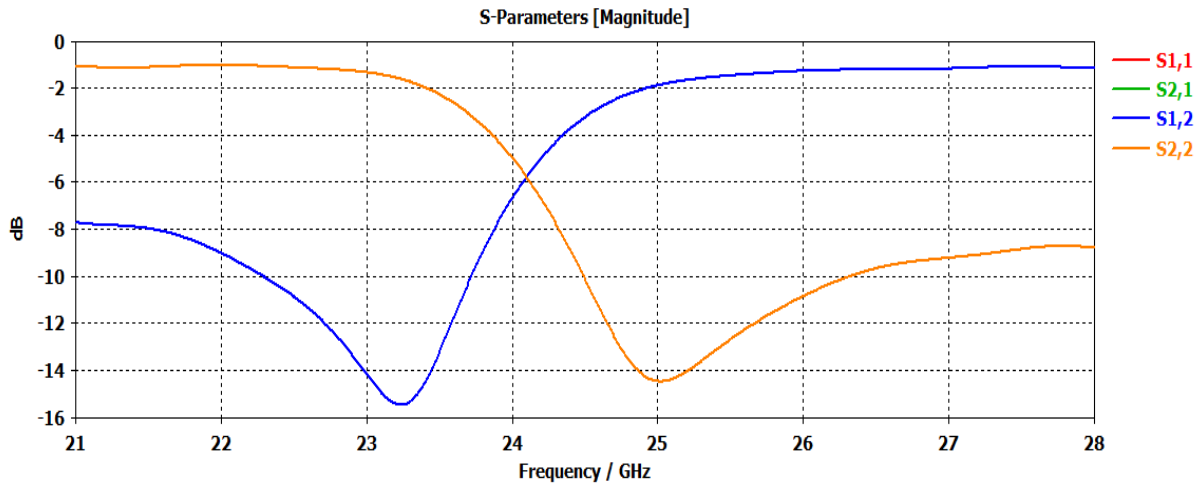


Fig. 12 Magnitude Plot of S-parameter v/s Frequency of designed SSRR- metamaterial

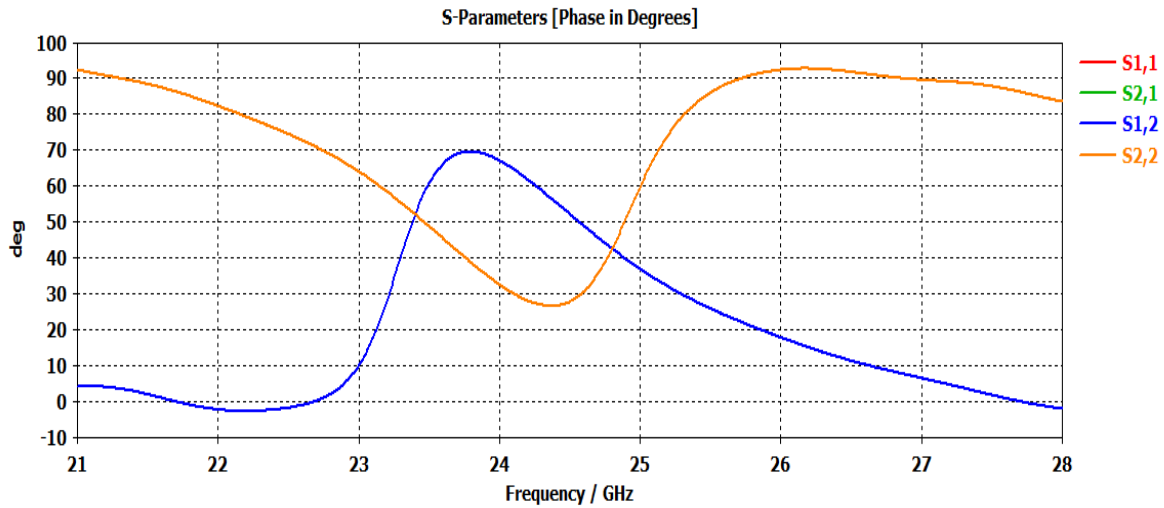


Fig. 13 Phase Plot S-parameter v/s Frequency of designed SSRR-metamaterial

S-parameter for the designed SSRR-metamaterial is used to confirm its double negative character using Matlab. Figure 14 depicts the acquired results and demonstrates that

permittivity and permeability are both negative around 24 GHz.

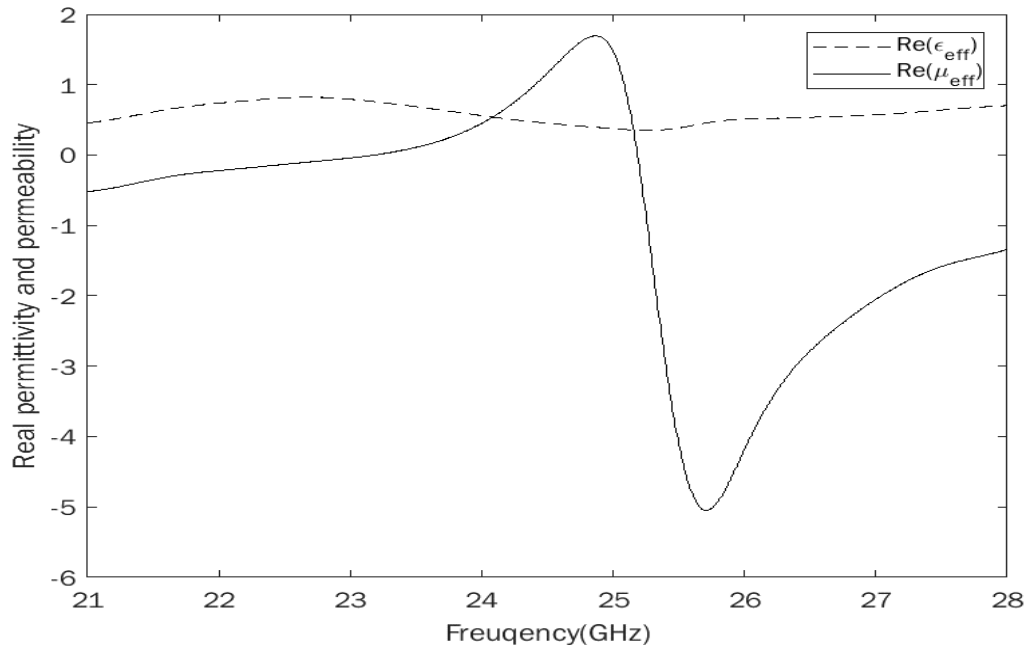


Fig. 14 Plot of Real Permittivity and Permeability V/S Frequency of Designed SRR Structure.

### 3.5. Design and analysis of a 2-port Multiple Antenna System loaded with Split Ring Resonator

A 2x2 Multiple Antenna System constructions with an SSRR-metamaterial is shown in Figure 15. As seen in Figure 15, 1x7 SSRR-metamaterial are positioned between microstrip patch antennas, with a separation of  $\lambda/4$ . Figure 16 illustrates the transmission coefficient of a 2-port Multiple Antenna system with an SSRR-metamaterial with a slotted ground structure is -33.89dB, with the antenna spacing is  $\lambda/4$ . By using far-field patterns, the envelope correlation

coefficient is assessed. When compared to the ECC value achieved using DGS as the decoupling structure, shown in Figure 17, the obtained value of ECC, which is shown at 0.0002, is less than 0.004. The diversity gain achieved by the two-port Multiple Antenna system with the SSRR-metamaterial with slotted ground decoupling structure is around 9.99dB, as shown in Figure 18. Figure 19 displays the Mean Effective Gain of the 2-port Multiple Antenna system with SSRR-metamaterial with the slotted ground. The far-field pattern is used to evaluate the MEG -3dB.

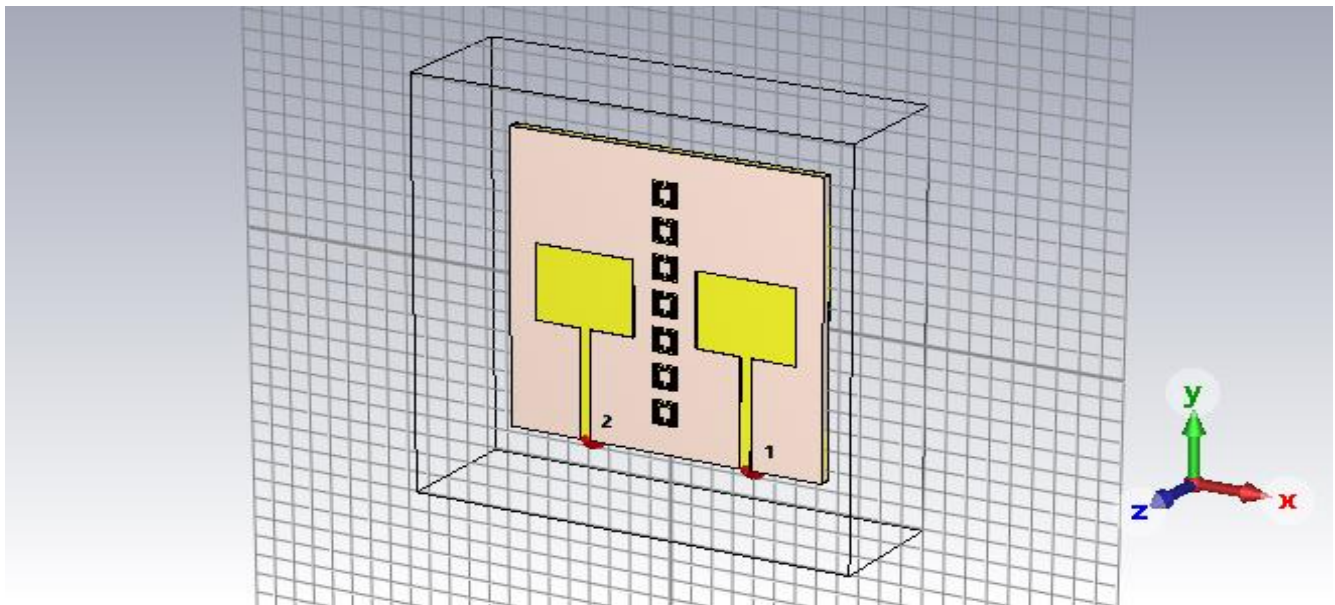


Fig. 15 2-Port Multiple Antenna loaded with SSRR-metamaterial

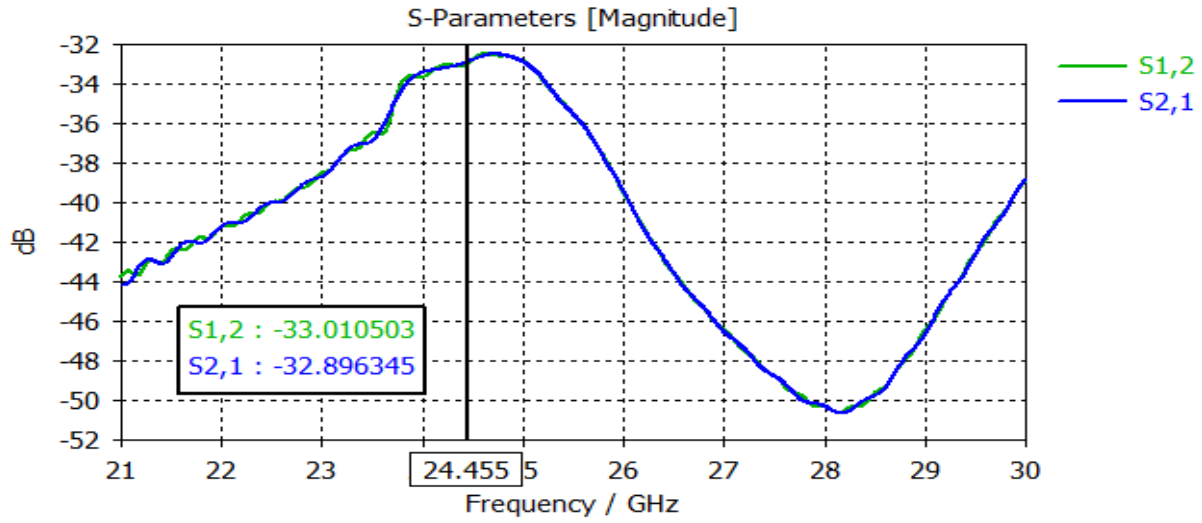


Fig. 16 S12, S21 of SSRR with Slotted ground loaded 2-port Multiple Antenna system

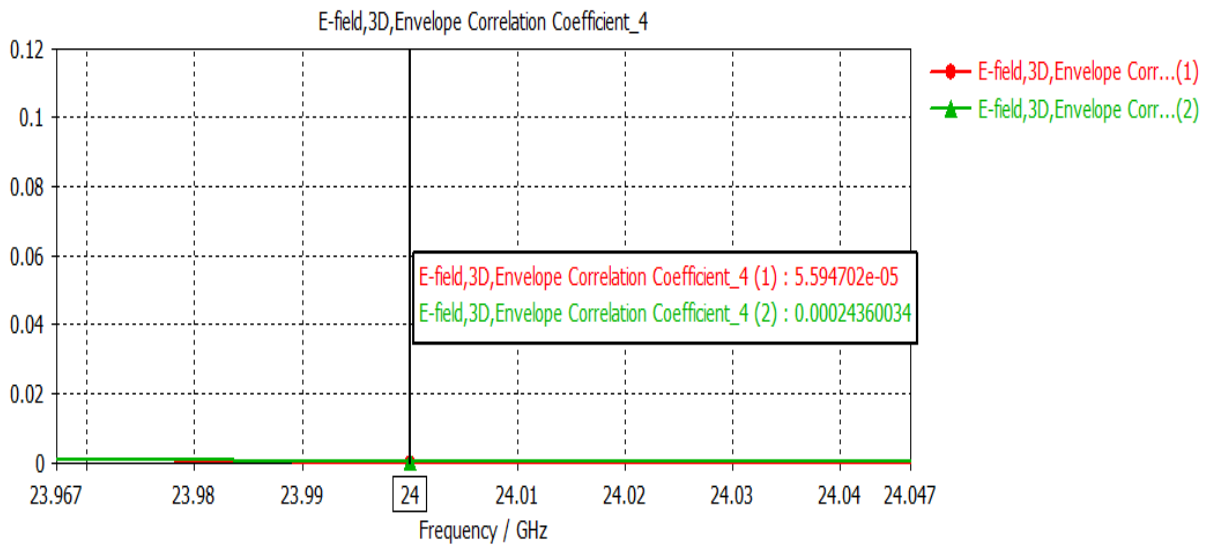


Fig. 17 Envelope Correlation Coefficient of SSRR with Slotted ground loaded 2-port Multiple Antenna

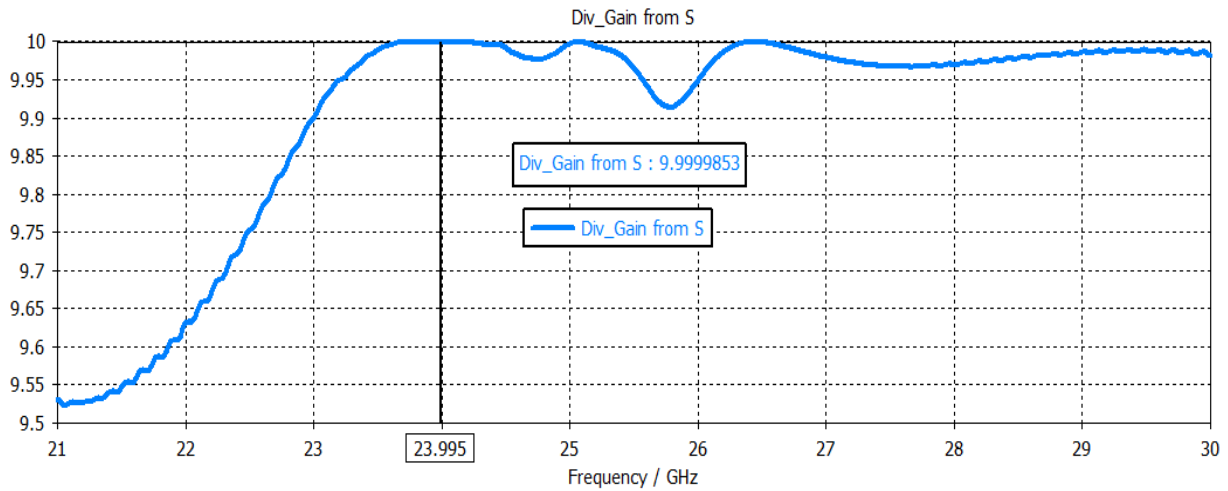


Fig. 18 Diversity Gain of SSRR with Slotted ground loaded 2-port Multiple Antenna system.

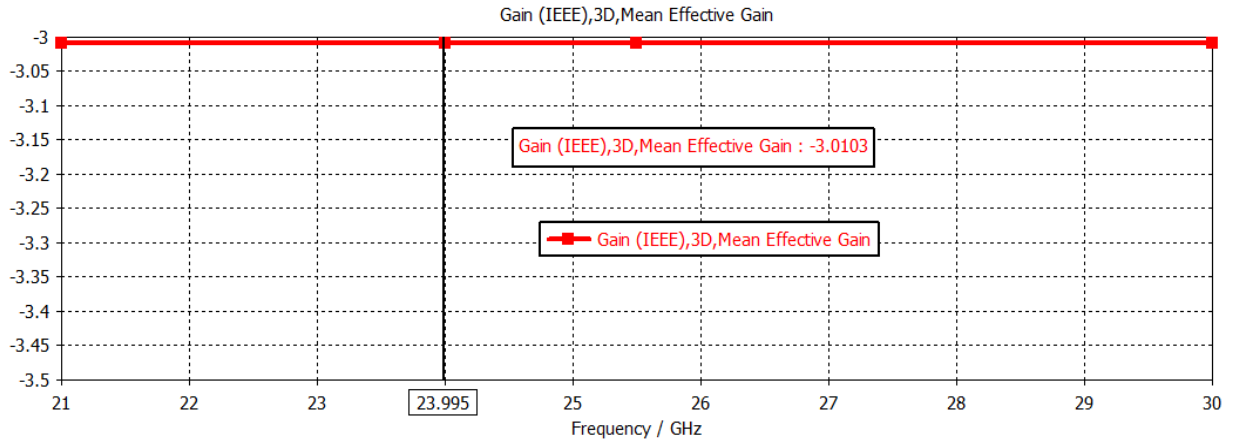


Fig. 19 Mean Effective Gain of SSRR with Slotted ground loaded 2-port Multiple Antenna system

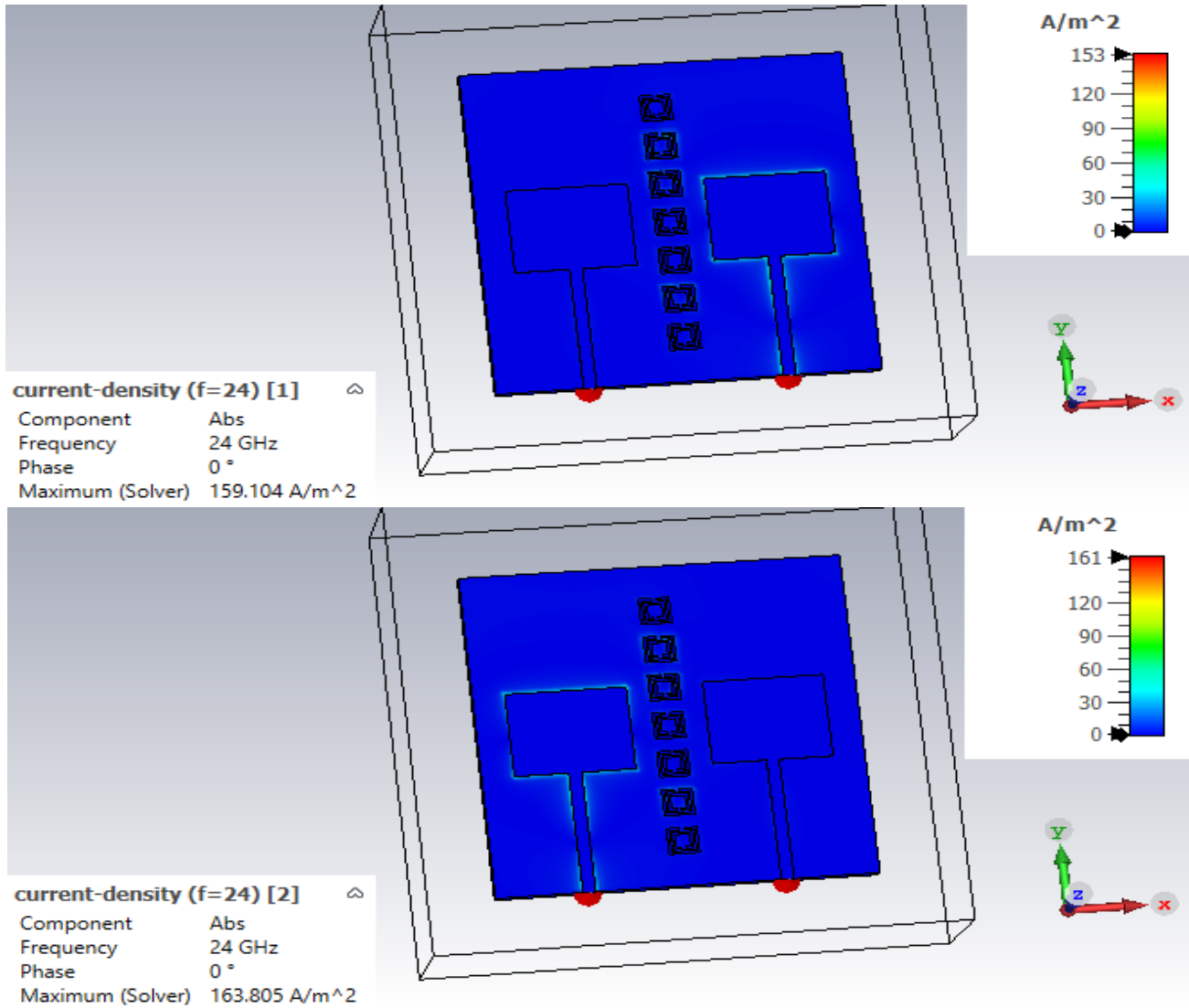


Fig. 20 Surface Current Density of SSRR with Slotted ground loaded 2-port Multiple Antenna systems

Surface Current Density of SSRR with Slotted ground loaded 2-port Multiple Antenna system. When either port is activated, Figure 20 depicts the surface current density. Figure 20 shows that the split ring resonator contributes to the strong isolation between the microstrip patch antennas.

The far-field patterns of the SSRR with slotted ground structure loaded, 2-port multiple antennae are shown in

Figure 21. The flown patterns across two principal planes for  $\phi=0$  and  $\phi=90$  are taken. It is observed that the major lobe for  $\phi=0$  for element-1 is around  $-13^\circ$  and for  $\phi=90$  along  $-6^\circ$ . For the radiating element -2, the main lobe is along  $+13^\circ$  for  $\phi=0$  and for  $\phi=90$  along  $-6^\circ$ . As depicted in Figure 20, the system exhibits a good pattern diversity characteristic compared to the structure discussed in section 4.

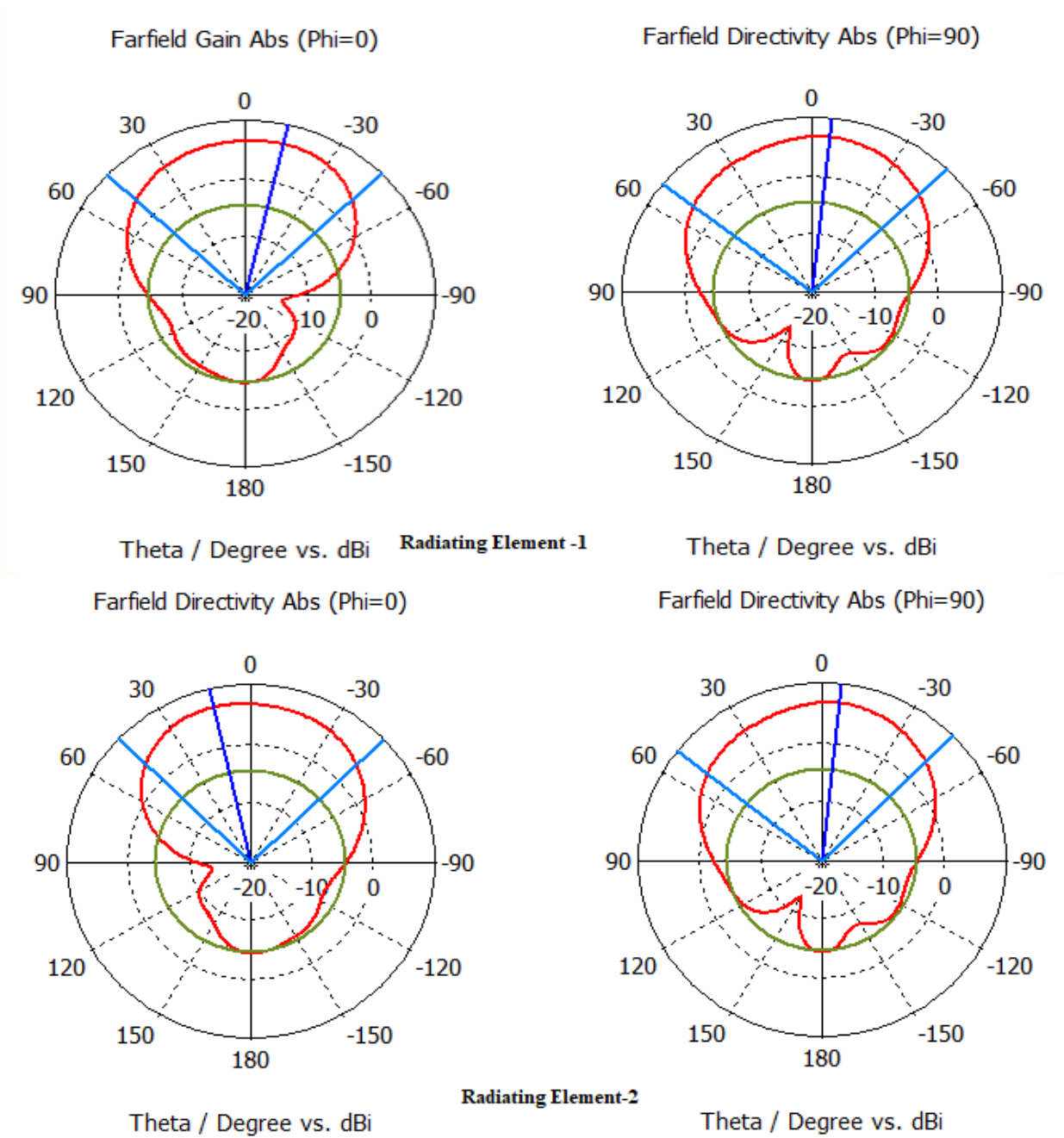


Fig. 21 Far Field Pattern of SSRR with Slotted ground loaded 2-port Multiple Antenna system

#### 4. Conclusion

This work aims to fit the 2-port Multiple Antenna operating at 24GHz, with high isolation between the elements and better performance. In order to meet the requirement, two decoupling strategies, namely slotted ground and square split ring resonator with the slotted ground, were introduced. The structures acted as decoupling elements and were responsible for increasing the isolation and minimising the mutual coupling between the antenna elements. The spacing between the antenna elements is decremented from  $\lambda/2$  to  $\lambda/4$ . The Multiple Antenna system metrics ECC is 0.0002 and 0.004 for SSRR-metamaterial and slotted ground structure, respectively. The far-field patterns for slotted ground alone exhibit low pattern diversity compared with SSRR-metamaterial and slotted ground structure. Thus, when SSRR-metamaterial is combined with a slotted ground structure, a 2-port Multiple Antenna system performs better than one with a slotted ground structure alone. Although adopting a deficient/slotted ground structure

appears straightforward, it reduces the antenna's radiating effectiveness/efficiency.

For the current millimeter wave communication, a compact antenna system is required. This proposed work can be extended to the NxN multiple antenna systems; with the proper decoupling structure, more antennae can be placed there by maintaining the system's performance. The decoupling structure allows the antenna placement with a spacing less than  $\lambda/2$ , resulting in more antennae on one single substrate.

Since the radiating element and the feed structure are on the same substrate, there are chances of discontinuity in the feed line that may lead the feed line itself to radiate. To overcome this, one can separate the feed line and radiating element. A multi-layer substrate can achieve it, wherein one layer is dedicated to the feed line and the other to radiating elements.

#### References

- [1] Sakli H, Abdelhamid C, Essid C, and Sakli N, "Metamaterial-Based Antenna Performance Enhancement for MIMO System Applications," *IEEE Access*, vol. 9, pp. 38546–38556, 2021. Crossref, <http://doi.org/10.1109/ACCESS.2021.3063630>
- [2] Garg P, and Jain P, "Isolation Improvement of MIMO Antenna Using a Novel Flower Shaped Metamaterial Absorber at 5.5ghz Wimax Band," *IEEE Transactions on Circuits and Systems*, vol. 67, no. 4, pp. 675-679, 2020. Crossref, <http://doi.org/10.1109/TCSII.2019.2925148>.
- [3] Wang Z, Zhao L, Cai Y, Zheng S, and Yin Y, "A Meta-Surface Antenna Array Decoupling (MAAD) Method for Mutual Coupling Reduction in a MIMO Antenna System," *Scientific Reports*, vol. 8, pp. 3152-3159, 2018. Crossref, <https://doi.org/10.1038/s41598-018-21619-z>
- [4] Xue C.D, Zhang X.Y, Cao Y.F, Hou Z, and Ding C.F, "MIMO Antenna using Hybrid Electric and Magnetic Coupling for Isolation Enhancement," *IEEE Transactions on Antennas and Propagation*, vol. 65, pp. 5162-5170, 2017. Crossref, <https://doi.org/10.1109/TAP.2017.2738033>
- [5] Yang C, Kim J, Kim H, Wee J, Kim B, and Jung C, "Quad-Band Antenna with High Isolation MIMO and Broadband SCS for Broadcasting and Telecommunication Services," *IEEE Antennas and Wireless Propagation Letters*, vol. 9, pp. 584-587, 2010. Crossref, <https://doi.org/10.1109/LAWP.2010.2053515>
- [6] RubayaKhatun, Mahfujur Rahman, and Abu Zafor Md. Touhidul Islam, "Design of a Compact Rectangular Microstrip Patch Antenna for 2.45 GHz ISM Band," *International Journal of Recent Engineering Science*, vol. 8, no. 3, pp. 30-35, 2021. Crossref, <https://doi.org/10.14445/23497157/IJRES-V8I3P105>
- [7] Larsson E.G, Edfors O, Tufvesson F, and Marzetta T.L, "Massive MIMO for Next Generation Wireless Systems," *IEEE Communications Magazine*, vol. 52, pp. 186-195, 2014. Crossref, <https://doi.org/10.1109/MCOM.2014.6736761>
- [8] Pei T, Zhu L, Wang J, and Wu W, "A Low-Profile Decoupling Structure for Mutual Coupling Suppression in MIMO Patch Antenna," *IEEE Transactions on Antennas and Propagation*, vol. 69, no. 10, pp. 6145-6153, 2021. Crossref, <https://doi.org/10.1109/TAP.2021.3098565>.
- [9] Tiwari R.N, Singh P, Kumar P, and Kanaujia B.K, "High Isolation 4-Port UWB MIMO Antenna with Novel Decoupling Structure for High Speed and 5G Communication," *In Proceedings of the 2022 International Conference on Electromagnetics in Advanced Applications (ICEAA)*, Cape Town, South Africa, pp. 336-339, 2022. Crossref, <https://doi.org/10.1109/ICEAA49419.2022.9900029>
- [10] Ghalib A, Sharawi M.S, "TCM Analysis of Defected Ground Structures for MIMO Antenna Designs in Mobile Terminals," *IEEE Access*, vol. 5, pp. 19680–19692, 2017. Crossref, <https://doi.org/10.1109/ACCESS.2017.2739419>
- [11] Pan B.C, Cui T.J, "Broadband Decoupling Network for Dual-Band Microstrip Patch Antennas," *IEEE Transactions on Antennas and Propagation*, vol. 65, pp. 5595-5598, 2017. Crossref, <https://doi.org/10.1109/TAP.2017.2742539>
- [12] Khalid M, IffatNaqvi S, Hussain N, Rahman M, Mirjavadi S.S, Khan M.J, and Amin Y, "4-Port MIMO Antenna with Defected Ground Structure for 5G Millimeter Wave Applications," *Electronics*, vol. 9, no. 71, 2020. Crossref, <https://doi.org/10.3390/electronics9010071>

- [13] Samir Salem Al-Bawri, Hui Hwang Goh, Md Shabiul Islam, Hin Yong Wong, Mohd Faizal Jamlos, Adam Narbudowicz, Muzammil Jusoh, Thennarasan Sabapathy, Rizwan Khan and Mohammad Tariqul Islam, "Compact Ultra-Wideband Monopole Antenna Loaded with Metamaterial," *Sensors*, vol. 20, no. 3, pp. 796, 2020. Crossref, <https://doi.org/10.3390/s20030796>
- [14] Ananda Kumar Behera, Debasis Mishra, S Nallusamy, Diptimayee Konhar, and Suvendu Narayan Mishra, "Fibonacci Series-Motivated Sequential-Elliptical-Pyramid Slotted Microstrip Antenna with C-Band and X-Band Isolation Features," *International Journal of Engineering Trends and Technology*, vol. 70, no. 8, pp. 118-125, 2022. Crossref, <https://doi.org/10.14445/22315381/IJETT-V70I8P211>
- [15] Yadgar I. Abdulkarim, Lianwen Deng, Heng Luo, Shengxiang Huang, Muharrem Karaaslan, Olcay Altıntaş, Mehmet Bakır, Fahmi F. Muhammadsharif, Halgurd N.Awl, Cumali Sabah, and Khalid Saeed Lateef Al-badri, "Design and Study of a Metamaterial-Based Sensor for the Application of Liquid Chemicals Detection," *Journal of Materials Research and Technology*, vol. 9, no. 5, pp. 10291–10304, 2020. Crossref, <https://doi.org/10.1016/j.jmrt.2020.07.034>
- [16] Gangwar D, Das S, and Yadava R. L, "Gain Enhancement of Microstrip Patch Antenna Loaded with Split Ring Resonator Based Relative Permeability Near Zero as Superstrate," *Wireless Personal Communications*, vol. 96, no. 2, pp. 2389–2399, 2017. Crossref, <https://doi.org/10.1007/s11277-017-4303-3>
- [17] Patel S. K, Argyropoulos C, and Kosta Y. P, "Broadband Compact Microstrip Patch Antenna Design Loaded by Multiple Split Ring Resonator Superstrate and Substrate," *Waves in Random and Complex Media*, vol. 27, no. 1, pp. 92–102, 2017. Crossref, <https://doi.org/10.1080/17455030.2016.1203081>
- [18] M. Shahidul Islam, M. Samsuzzaman, G. K. Beng, N. Misran, N. Amin and M. T. Islam, "A Gap Coupled Hexagonal Split Ring Resonator Based Metamaterial for S-Band and X-Band Microwave Applications," *IEEE Access*, vol. 8, pp. 68239–68253, 2020. Crossref, <https://doi.org/10.1109/ACCESS.2020.2985845>.
- [19] Mr. Navneet Kumar, and Dr. Narinder Sharma, "The Various Feeding Techniques of Microstrip Patch Antenna Using HFSS," *SSRG International Journal of Electronics and Communication Engineering*, vol. 6, no. 6, pp. 23-29, 2019. Crossref, <https://doi.org/10.14445/23488549/IJECE-V6I6P106>
- [20] Jain A, and Yadav S. K, "Design and Analysis of Compact 108 Element Multimode Antenna Array for Massive MIMO Base Station," *Progress In Electromagnetics Research C*, vol. 61, pp. 179–184, 2016. Crossref, <https://doi.org/10.2528/PIERC15110502>
- [21] Saurabh A. K, and Meshram M. K, "Compact Sub-6 Ghz 5G-Multiple-Input-Multiple-Output Antenna System with Enhanced Isolation," *International Journal of RF and Microwave Computer Aided Engineering*, vol. 30, pp. e22246, 2020. Crossref, <https://doi.org/10.1002/mmce.22246>
- [22] M. Firoz Ahmed, Abu Zafor Md. Touhidul Islam, and M. Hasnat Kabir, "Design of a Ultra-Wideband Rectangular Patch Microstrip Antenna with Improved Bandwidth," *International Journal of Recent Engineering Science*, vol. 8, no. 5, pp. 6-12, 2021. Crossref, <https://doi.org/10.14445/23497157/IJRES-V8I5P102>
- [23] Geetharamani G, and Aathmanesan T, "Design of Metamaterial Antenna for 2.4 Ghz Wi-Fi Applications," *Wireless Personal Communications*, vol. 113, pp. 2289–2300, 2020. Crossref, <https://doi.org/10.1007/s11277-020-07324-z>
- [24] Wang B.X, He Y, Lou P, and Xing W, "Design of a Dual-Band Terahertz Metamaterial Absorber Using Two Identical Square Patches for Sensing Application," *Nanoscale Advances*, vol. 2, pp. 763–769, 2020. Crossref, <https://doi.org/https://doi.org/10.1039/C9NA00770A>
- [25] Al-Hasan M. J, Denidni T. A, and Sebak A. R, "Millimeter-Wave Compact EBG Structure for Mutual Coupling Reduction Applications," *IEEE Transactions on Antennas and Propagation*, vol. 63, no. 2, pp. 823-828, 2015. Crossref, <https://doi.org/https://doi.org/10.1109/TAP.2014.2381229>
- [26] Oluseun Oyeleke Wikiman, OlabodeIdowu-Bismark, OluwafemiIlesanmi, Sadiq Thomas, Dyaji Charles Bala, "PIFA Antenna Design for MmWave Body Centric 5G Communication Applications," *SSRG International Journal of Electronics and Communication Engineering*, vol. 6, no. 4, pp. 6-10, 2019. Crossref, <https://doi.org/10.14445/23488549/IJECE-V6I4P102>
- [27] Bhattacharya A, Roy B, "Investigations on an Extremely Compact MIMO Antenna with Enhanced Isolation and Bandwidth," *Microwave and Optical Technology Letters*, vol. 62, pp. 845-851, 2020. Crossref, <https://doi.org/10.1002/mop.32084>
- [28] Yao J, Tchafa F. M, Jain A, Tjuatja S, and Huang H, "Far-Field Interrogation of Microstrip Patch Antenna for Temperature Sensing without Electronics," *IEEE Sensors Journal*, vol. 16, pp. 7053–7060, 2016. Crossref, <https://doi.org/10.1109/JSEN.2016.2597739>
- [29] Azeez A. R, Elwi T. A, and Al-Hussain Z. A. A, "Design and Analysis of a Novel Concentric Rings Based Crossed Lines Single Negative Metamaterial Structure," *Engineering Science and Technology, an International Journal*, vol. 20, pp. 1140–1146, 2017. Crossref, <https://doi.org/10.1016/j.jestch.2016.11.010>
- [30] Sharawi M. S, Hassan A. T, and Khan M. U, "Correlation Coefficient Calculations for MIMO Antenna Systems: A Comparative Study," *International Journal of Microwave and Wireless Technologies*, vol. 9, no. 10, pp. 1991–2004, 2017. Crossref, <https://doi.org/10.1017/S1759078717000903>